STARS

Electronic Theses and Dissertations, 2004-2019

2017

Implementation of Optical Interferometry and Spectral Reflectometry for High Fidelity Thin Film Measurements

Armando Arends-Rodriguez
University of Central Florida

Part of the Aerodynamics and Fluid Mechanics Commons

Find similar works at: https://stars.library.ucf.edu/etd

University of Central Florida Libraries http://library.ucf.edu

STARS Citation

IMPLEMENTATION OF OPTICAL INTERFEROMETRY AND SPECTRAL
REFLECTOMETRY FOR HIGH FIDELITY THIN FILM MEASUREMENTS

by

ARMANDO ANDRE ARENDS-RODRIGUEZ
B.S. University of Central Florida, 2015

A thesis submitted in partial fulfillment of the requirements
for the degree of Master of Science
in the Department of Mechanical and Aerospace Engineering
in the College of Engineering and Computer Science
at the University of Central Florida
Orlando, Florida

Spring Term
2017

Major Professor: Shawn A. Putnam

ABSTRACT

An in-house reflectometer/interferometer has been built to investigate the varying curvature and thickness profiles in the contact line region of air, acetone, iso-octane, ethanol, and water on various types of substrates. Light intensity measurements were obtained using our reflectometer/interferomter and then analyzed in MATLAB to produce thickness and curvature profiles. The apparatus is based on the principle of a reflectometer, consisting of different optical elements, probe, light source, and spectrometer. Our reflectometer/interferomter takes measurements in the UV-Vis-IR range (200nm-1000nm). This range is achieved by using a light source that has both a deuterium light (190nm-800nm), a tungsten halogen light (400nm-1100nm), a Metal-Core Printed Circuit Board LED (800nm-1000nm) and a Metal-Core Printed Circuit board cold white LED (400nm-800nm, 6500 K). A UV-VIS-IR spectrometer reads the light response after light is focused on the region of interest. Then a CCD camera (2448x2048) records the profiles for image analyzing interferometry. The readings were then validated based on results in the literature and studies with cylindrical lens samples.

ACKNOWLEDGMENTS

TABLE OF CONTENTS

LIST OF FIGURES

LIST OF TABLES

CHAPTER 1: INTRODUCTION

Background

Reflectometry and interferometry are effective techniques that are extensively used due to their critical importance in nearly all the fields of science and engineering [1]–[7]. Throughout the years it has been proven that reflectometers and interferometers are effective tools that can characterize the optical properties of solid and liquid thin films [8]–[14]. Basically, a reflectometer measures the properties of a medium. This is achieved when light waves reflect at a specific interface. Waves travel through a medium and when they find a break, a portion of the energy reflects into the insertion point. An interferometer is a device that measures the interference of fringes to obtain accurate measurements of distance. The degree of which light is phase shifted through a medium, results in constructive and destructive interference. Our apparatus detects the reaction of said interferences and provides information to characterize the medium. Interactions between thin liquid films, vapor, and solid surfaces have been widely studied because of their meaning to balance and non-balance singularities [15]–[17].

Research focus and motivation

The focus of this technique is to observe and record the response of light on and through a thin film. Currently, there are individual reflectometers and interferometers. In the presence of a thin film meniscus and an extended absorbed film, two measurements are needed simultaneously. The novelty of our apparatus is that it combines the reflectometer with a camera imaging system to read interference like an interferometer would do. Meniscus studies help in the optimization of

design and use of microscale systems, fluid flow, and stability in an extended meniscus [18]. These studies are a direct application for this instrument.
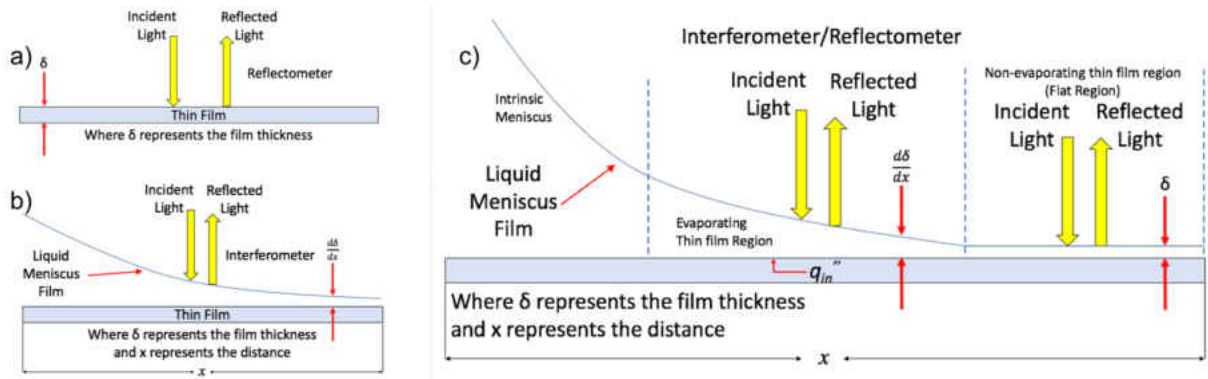
Figure 1: a) Representation of a reflectometer for thin film measurements. b) Representation of an interferometer to read curvature profiles. c) Combination of both a reflectometer and an interferometer.

Figure 1 is an example of a liquid film on a solid film where a) shows that a reflectometer is used for measuring thin films, b) shows an interferometer is used to measure curved films c) shows the combination of a reflectometer and an interferometer where the interferometer is used in the curved and the reflectometer is in the flat region where the film is flat.

The region of interest of the camera is slightly larger than the reflectometer response region to ensure accurate data recording region. Once the camera and light are focused, a grayscale image is obtained. The image is then processed and analyzed through a code on MATLAB to obtain a film thickness. Once the thickness is obtained at various x locations curvature profile can be calculated. After the curvature profile is obtained, the heat transfer properties of the liquid thin film can be projected.

We describe a reflectometry that implements both reflectometry and interferometry at the into a single instrument for simultaneous measurements of curvature and thin films. This

instrument will be used to measure heat transfer properties of different types of films air and liquid solid surfaces. This technique builds on our expertise in measuring heat transfer properties of different liquid substances. In comparison to traditional reflectometry methods, we include a spectrometer and camera imaging system for interferometry to conclude curvature properties of diverse films.

CHAPTER 2: EXPERIMENT MATERIALS

To run a curvature experiment in our spectrometer the following components are needed: One light source to look in the UV-VIS and another light source to look in the IR. To achieve this range, a light source consisting of deuterium and tungsten halogen lights, a combined light source of IR and white light, 4 kinds of focusing optics, a spectrometer in the UV-VIS-IR range to read the response of the reflected light, a reflective objective lens to focus the light in the sample and then get a response from it read by the spectrometer, a silver mirror with a hole in it to reflect light, and two electronic translational stages to move the sample in the x and y direction. A computer with LabView was used to control the camera, spectrometer, and stages. To obtain curvature profile measurements a MATLAB code that reads images, fringes and does signal analysis was used.
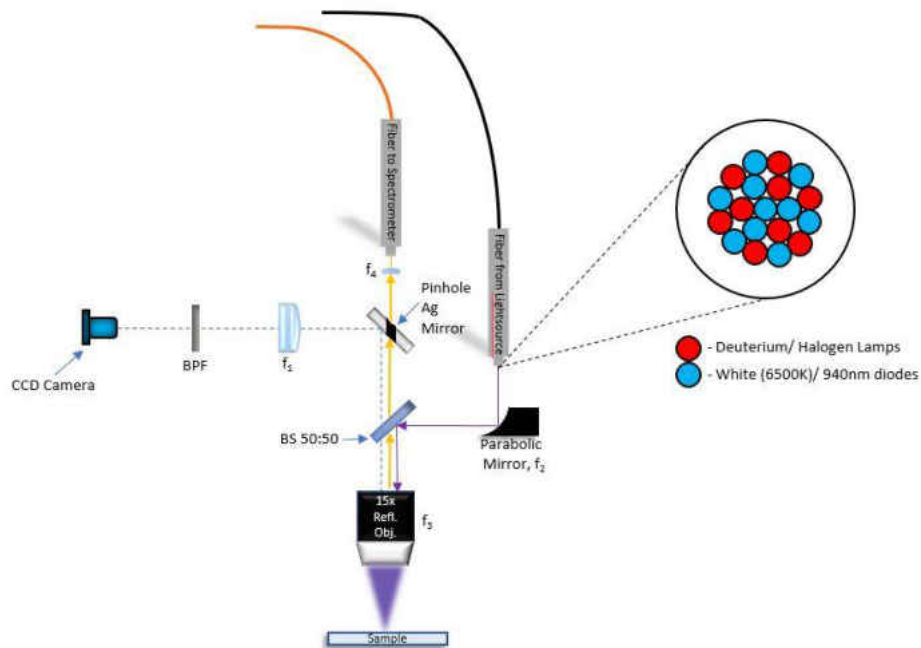
Figure 2: Optical setup of reflectometer/interferomter apparatus

<u>Light source and spectrometer/interferomter</u>

A light source (Ocean Optics DH-2000) with a combination of deuterium (190nm-800nm range) and tungsten (400nm-1100nm) halogen light was used. The total range of this light source is 190nm-1100nm. The nominal bulb powers are 26 Watts for deuterium and 20W for tungsten halogen. An IR ThorLabs M940D2 LED on a Metal-Core Printed Circuit Board (MCPCB) designed to have a high-power output in a small package with a nominal wavelength of 940nm (range is 800nm to1000nm, minimum power is 800mW, and typical emitted power is 1000mW) was also used. A ThorLabs MCWHD3 6500 K white light LED MCPCB (400nm-800nm range, LED output power = min: 2350mW, typical: 2700mW) was combined with the ThorLabs IR LED into a single output light source. Then the 4 different types of lights come out from the two combined light sources into a 2 input to 1 input ThorLabs optical fiber BF19Y2H02 (250nm –

1200nm range) which guides the lights to the desired location. Ten fibers guide the light from the combined IR LED and cold white LED, and nine fibers guide the light into a combined nineteen fiber single light output to the desired location. Figure 2 shows the tip of the combined fibers that output the light. To obtain the reflected signal from a sample an HR400 Ocean Optics spectrometer was used (wavelength range = 190nm-1100nm, integration time = 4ms-20sec (continuous); 10ms-4ms (shutter), Optical resolution = ~0.02-8.4nm FWHM).

Focusing optics and filters

A total of four different focusing lenses were used and one filter was used as follows: a Thor Labs 25mm x 36mm 50/50 UVFS plate beam splitter coated for 250nm-450nm, in which the light from the light sources reflects into the reflective objective and transmits the reflected light form the surface into the spectrometer. An Edmunds Optics 15x infinite conjugate objective reflective (UV enhanced aluminum coated, working distance = 23.75mm, f_3 = 13.3mm, wavelength range = 200nm-11000nm) focuses the collimated light into the sample for the reflection measurements. An Infinite conjugate Mitutoyo Plan Apochromat Objective 10x lens 378-803-3 (Numerical aperture = 0.28, Working Distance = 34mm, and Focal, and a Parfocal Length = 95mm). A Thor Labs ½ in 90° Off-Axis Parabolic mirror (UV Enhanced aluminum coating, reflected f_2 = 15mm, parental focal length = 7.5mm) was used to collimate the incident light into the reflective objective. Finally, a ThorLabs UVFS Plano convex lens (Diameter = 12.7mm, f_4 = 20mm) was used to collimate the reflected light into the spectrometer fiber for spectral readings.

<center>Samples</center>

To accomplish the desired measurements, multiple samples were used to characterize the optical setup. A pure silicon (Si) substrate was used to calculate the emitted signal, $I_o(\lambda_i)$, using known literature values for the reflection spectrum of Si, $R_{Si}(\lambda_i)$. This process was repeated for three calibration samples including the fore mentioned Si as well as silicon dioxide (S_iO_2) on Si, unprotected gold (Au), and germanium (Ge). The calibration of reflection for all samples can be seen below in results chapter. To start characterizing the apparatus, a basic experiment consisting of a Fisher Scientific microscope cover glass S17522 Dimensions = 25mm x 25mm, thickness = 0.17mm-25mm) and two Thermo Fisher Scientific plain thick slides NO. 3048 (Dimensions = 3in x 1in, Thickness = 1.2mm) glasses was performed to create an air wedge at an angle θ to read equally spaced fringes. The microscope cover glass was placed between the two slides to create an angle. Four different types of concave lenses with different curvature profiles were observed. The difference in curvature of these lenses gives the observer different fringe frequencies in which the fringe spacing is analyzed to obtain the curvature profile. Lens$_1$ is an Edmund Optics cylindrical lens 68031 (Dimensions = 12.5mm x 25mm, f_1 = 20mm, Uncoated, R_1 = 10.34mm). Lens$_2$ is an Edmunds Optics cylindrical lens 68033 (Dimensions = 12.5mm x 25mm, f_2 = 50mm, Uncoated, R_2 = 25.84mm). Lens$_3$ is an Edmunds Optics cylindrical lens 68035 (12.5mm x 25mm, f_3 = 100mm, Uncoated, R$_3$ = 51.68mm). To mimic a meniscus profile, a Polydimethylsiloxane (PDMS) was made in-house molded around Lens$_1$ since it has the most curvature. The molded PDMS sample has the same radius/curvature as lens$_1$, so it can be compared to Lens$_1$ and show the same curvature profile. The results section shows an accurate comparison of the curvature profile

<center>7</center>

of the lens molded with PDMS and the PDMS sample. To show circular fringes (Newton Rings) a ThorLabs cylindrical plano convex lens (D_4 = 25.4mm, f_4 = 50mm) was observed.

Imaging system

The curvature profiles were observed using an imaging system that consisted of, a Point Grey CCD camera (resolution = 2448x2048, frame rate = 8FPS, 5 megapixels) to obtain pictures of different profiles in grayscale images for analysis. An achromat (f_1 = 120mm) for better visibility, and to look at the peak of interest with the camera. A 1in ThorLabs band pass filter FB600-10 (center wavelength = 660nm, Bandwidth = 10 nm, Blocking Regions = 200nm–648nm and 672nm-1200nm) was used to obtain images at a wavelength 656nm. Another ThorLabs band pass filter FB450-10 (center wavelength = 450nm, Bandwidth = 10 nm, Blocking Regions = 200nm–438nm and 462nm-1200nm) was used to obtain images at a wavelength of 450nm. The imaging system was characterized using an Edmund Optics reticle that has lines with 50um spacing in between them.

CHAPTER 3: EXPERIMENT DESIGN AND CONFIGURATION

Solid thin film scheme

When any kind of wave strike a surface like a mirror, newly formed waves bounce away from the that surface. This occurrence is called reflection. For reflection to happen, there must be two mediums with varying indices of refraction, in most cases in optics they are air and a type of metal or glass. The incident light or incident energy is the light that comes into the surface. Part of this light is transmitted and some of it is reflected. Figure 3 shows light reflecting from an air-glass sample.
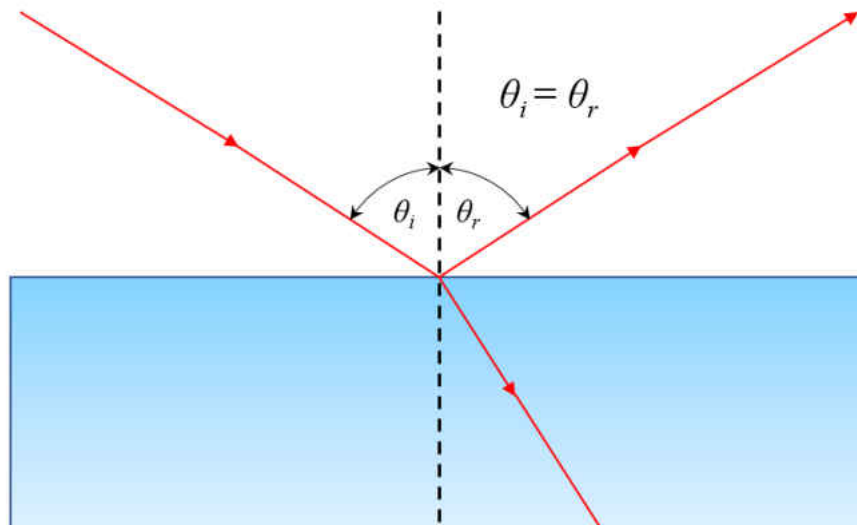
Figure 3: Representation of the incident light θ_i equal to the angle of the reflected light θ_r.

Angle θ_i is the angle between an incident beam of light and the normal line, normal line being perpendicular to the sample's surface. This angle is called the angle of incidence and the plane that is outlined is called the plane of incidence of the two lines. The reflected beam is across

the plane of incidence and produces an angle θ_r with the normal plane like the Figure 3 shows. The following equation shows this occurrence [19]:

$$\theta_i = \theta_r \qquad (1)$$

The refractive index n is the ratio of the velocity of light in a vacuum c_v and the velocity of light in a specified medium v_m is shown in Equation 2 below [19]:

$$n = \frac{c_v}{v_m} \qquad (2)$$

In this instrument, light is reflected at a surface at normal incidence where $\theta_r = \theta_i = 0$. The reflected intensity of light $I(\lambda_i)$ for this instrument can be stated as follows in the equation 3 below:

$$I(\lambda_i) = \left(\frac{n_1(\lambda_i) - n_2(\lambda_i)}{n_1(\lambda_i) + n_2(\lambda_i)}\right)^2 I_o(\lambda_i) \qquad (3)$$

In this instrument two mediums are used to analyze the reflection of a sample, where n_1 is the refractive index of air and n_2 is the refractive index of the surface where the incident light is reflected from, λ_i is the single, specific wavelength of light and I_o the incident light intensity that comes into the surface of the sample. After the light reflects from the surface it is then focused into a spectrometer to obtain an intensity measurement per wavelength of the reflected light, $I(\lambda_i)$, which is then compared to the numerically calculated values of $I(\lambda_i)$ in Equation 3.

In the solid thin film scheme, one light source with two lamps and two LED's are focused into a solid thin film sample to obtain a reflection response reading. The schematic for this section is shown on Figure 2. The DH-2000 light source used was in the 200nm-1100nm range (Deuterium and Tungsten halogen), a ThorLabs LED was in the 800nm-1000nm and another ThorLabs LED was 6500 K white light. To guide the light from the two light sources to the desired location a

ThorLabs 2 to 1 optical fiber was used. Once, the light comes out of the fiber it reflects on a 90°

parabolic mirror $f_2 = 15$mm to collimate the light into the reflective objective. Light is then

reflected by a 50/50 UVFS Beam Splitter (250nm-450nm) into a 15x infinite conjugate objective

reflective (WD = 23.5mm and $f_3 = 13.3$mm) that focuses the light into the sample. Once light

reflects from the sample it goes back into the reflective objective through a collimating lens ($f_4 =$

20.1mm) and then to a spectrometer (190nm-1100nm) to read the reflected response. To look at

the regions of interest of the sample was mounted on a stepper motor stage controlled by a

LabView program.

<center>Liquid thin film meniscus scheme</center>

To characterize this setup one would have to go back to the basics of interference in thin

films. If an oil film on water is observed when the sun hits it, different colored fringes will be

noted. These different colored fringes represent the change in thickness of the oil film due to the

interference of the upper and lower parts part of the film. The difference in fringe colors occur

because of the different thicknesses of the film. These colors will cause interference at different

wavelengths observed at different points.

Consider the oil film mentioned before. When incident light hits the top of a medium at an

angle part of it reflects away from it. Since the speed of light is slower in any other medium

compared to air, there is a phase change in the light reflection. Some of the light travels through a

medium and is somewhat reflected from the bottom surface of the medium. If the incident light is

perfectly normal there will be no phase change. The light reflected at the top of a film will undergo

a 180 degree phase change and the light behind the film will not change phase and will interfere

<center>11</center>

destructively. At the edge of the oil film, interference undergoes a 180 degree change, the light will interfere destructively, which will look dark. In the other parts of the film where the oil is thicker the interference will be either constructive or destructive depending on the thickness of the film and wavelength, and will show different colors.

When a film of different thicknesses is observed with a single wavelength light, alternating fringes (dark and light gray in our setup) will show up in the image. The distance between these dark and light fringes tell how the thickness changes in respect to the path difference.
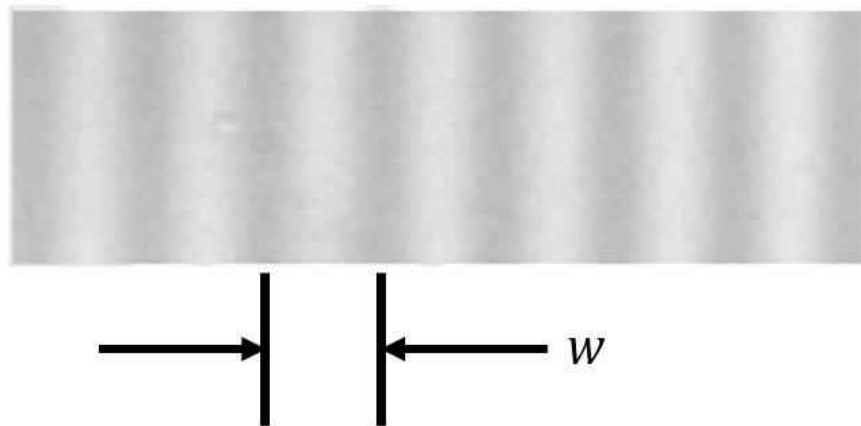
Figure 4: Separation of fringes of a constant angle air film similar.

The distance between two consecutive fringes needs to change by λ/2 for an almost perpendicular view, since the light must travel downward and upward. Where λ represents the wavelength of light in the medium of the wedge. In this case, the medium is air so the refractive index is approximately 1. The following equation expresses the separation between fringes [20].

$$W = \frac{\lambda}{2\theta} \qquad (4)$$

where, *W* represents the separation between two consecutive fringes, λ represents the wavelength of light through the medium observed, and θ represents the angle of the wedge.
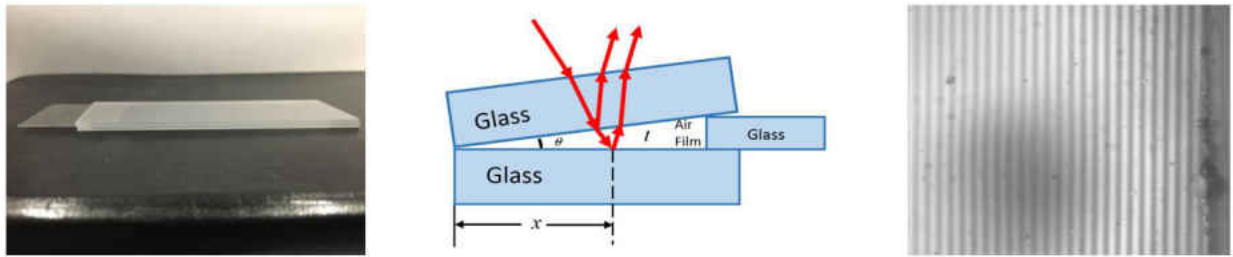
Figure 5: Representation of incident light through a wedge shape film of air between two flat (No curvature) glass substrates.

Figure 5 shows the interference of an air film between two microscope glasses. A basic experiment was performed to create an air wedge at an angle θ to read equally spaced fringes. The microscope cover glass was placed between the two slides to create an angle. Observing the glass from above alternating (black and white in our setup) equally spaces fringes can be seen. In this case, using Equation 4, the spacing between the fringes is equal since the angle remains constant as *x* changes.

A pattern interference can be observed in Figure 6 below, where light is reflected from an ambient air film between a round one inch spherical glass lens and a flat plane glass substrate.
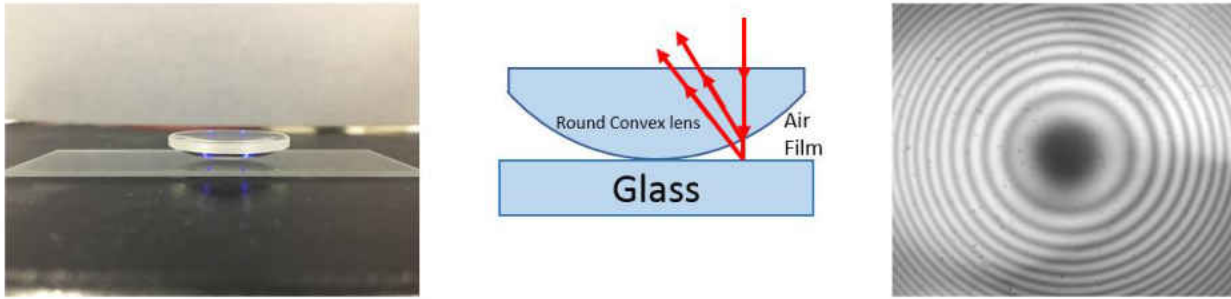
Figure 6: Representation of a film of air between a glass substrate and a round 1 inch convex lens with a constant curvature.

 These type of circular interference fringes are known as Newton Rings. Notice that in between the point of contact of the concave lens and bottom glass surface as the curvature increases the fringes get closer. The first ring occurs when the radius is half the wavelength of air contributing to a difference of phase of 180 degrees. As the curvature changes the phase changes to a total phase difference of 360 degrees, which at this point it is equal to a zero-phase change. The second ring occurs when the path difference is the wavelength of air. The following equation shows how the angle and frequency are a function of the radius:

$$\theta(r) \propto f(r) \qquad\qquad (5)$$

In a constant curvature round convex lens, like the one shown in Figure 6 above, where the angle θ is a function of the radius r, and f is the frequency of the fringes which are directly proportional the angle θ. As the radius increases, theta increases at the same rate as the frequency.

 The approach to observe cylindrical lenses is almost same as the circular convex lens mentioned above. The difference between these cylindrical lenses and the circular convex lens in Figure 6, is the shape. The curvature of cylindrical lenses changes in the x direction whereas the circular lens changes with the radius.

14
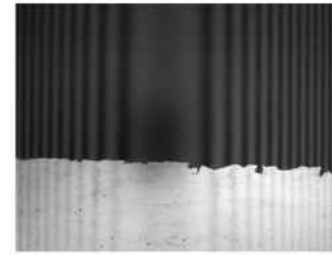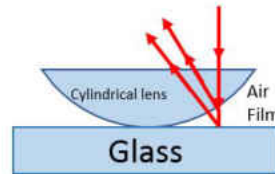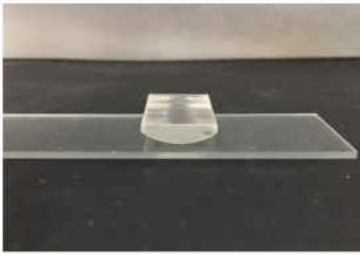
Figure 7: Representation of a film of air between a cylindrical convex and a flat plate

The interference pattern from the center of the cylindrical lens can be observed in Figure 7 (right). The following equation shows how the angle and frequency are a function of position (x):

$$\theta(x) \propto f(x) \tag{6}$$

Like the circular lens, as x increases from the contact region where the angle is zero, the spacing between the fringes is larger. Using Equation 4, as the angle increases the separation between the fringes is smaller resulting in a larger frequency.

In the experimental setup, various types of cylindrical lenses with different curvature profiles were observed. Figure 8 below shows the three different lenses observed.

$f_1 = 20\text{mm}$
$R_1 = 10.34\text{mm}$
Lens$_1$

$f_2 = 50\text{mm}$
$R_2 = 25.84\text{mm}$
Lens$_2$

$f_3 = 100\text{mm}$
$R_3 = 51.68\text{mm}$
Lens$_3$

Glass
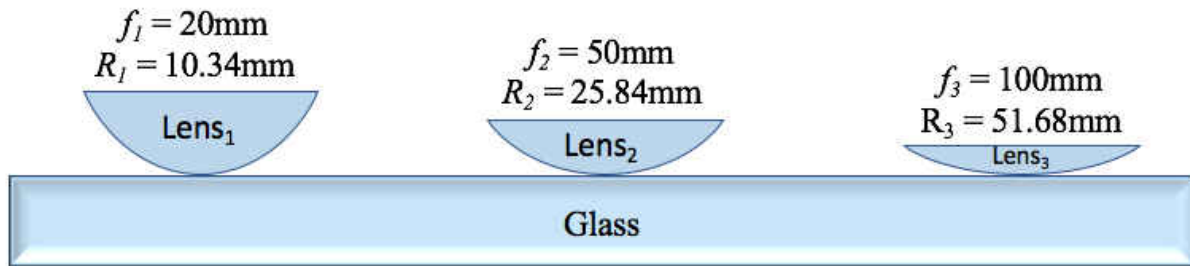
Figure 8: Lens profile, focal length, and radius of different lenses observed

The first, Lens$_1$, consisted of a focal length of 20mm and a radius of 10.34mm as shown in Figure 8. It can be observed in Figure 7 that the fringes are optically straight because the lens has a cylindrical geometry. In comparison to the fringes of the circular convex lens from Figure 6 above, it can be observed cylindrical lenses have straight fringes as opposed to fringes in circular lenses with circular fringes.

The second lens, Lens$_2$, consisted of a focal length 50mm and radius of 25.84mm as shown in Figure 8. This lens is a cylindrical lens like the previous lens mentioned above. The difference between this Lens$_2$ and the previous Lens$_1$ examined, is that this one has a different radius and focal length. The radius of Lens$_2$ is smaller and the focal length is shorter, meaning that the curvature profile is wider. It can be observed that the fringes of this Lens$_2$ are in the same orientation as the previous Lens$_1$ because the geometry is cylindrical.

The third lens, Lens$_3$, consisted of a focal length of 100mm and a radius of 51.58mm as shown in Figure 8. Lens$_3$ is cylindrical, like the two previous lenses described. Again, the difference between this lens and two previous lenses is that the focal length and radius are larger meaning that the curvature profile is smaller. According to Equation 4, this lens should have the largest separation between fringes and a smaller frequency since the air film is thinner.

The liquid meniscus is an important section of a fluid due to its heat transfer characteristics. Figure 1 in the introduction shows the different regions of a meniscus. The meniscus consists of three different regions, which are the absorbed, thin film (flat region), and intrinsic meniscus regions. Intermolecular interactions occur in the absorbed region of the film. The fluid between the thin film and the intrinsic meniscus region is where the heat flux occurs. This setup is a great approach to characterize heat transfer properties of liquid meniscuses of different fluids in the micro to nano scale. It is a tool that facilitates the measuring of thin films using both a CCD camera for the micron scale measurements and a spectrometer for the nano scale measurements.

CHAPTER 4: RESULTS AND DISCUSSION

Formulas

To characterize the film thickness of a sample, the measured response from the reflection of the gas or liquid sample, is detected by the spectrometer and then compared to previous literature data on that specific material. An overview of the approach for analysis is shown in Figure 9 below.
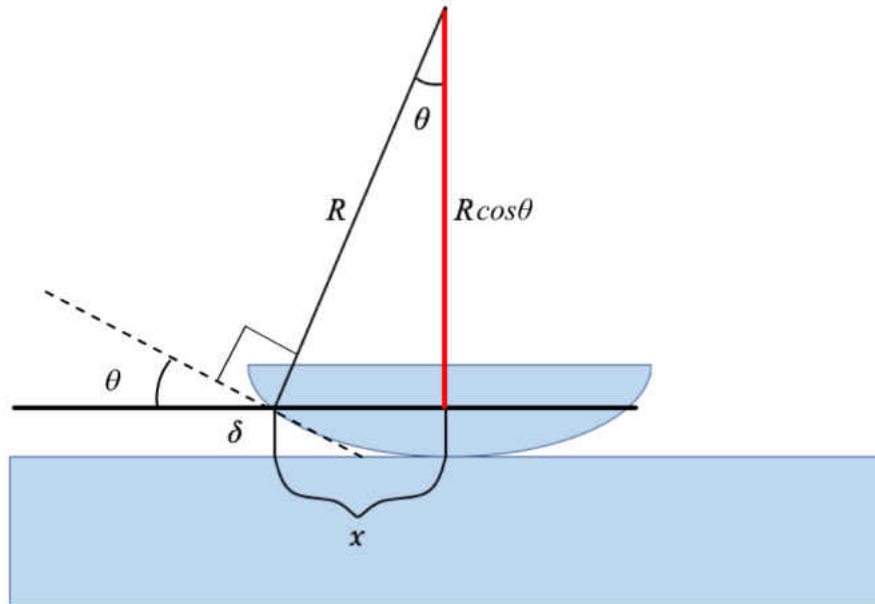
Figure 9: Overview of analysis

The thickness, δ, of a liquid or air film sample at a specific point can be estimated by the following equation [20]:

$$\delta = R - R\cos\theta = \frac{x^2}{2R} \qquad (7)$$

where $\delta(x)$ is film thickness at a specific x location, x is the distance from the contact point $\delta(0) = 0$, and the angle, θ, is the angle of the horizontal and the vapor film. The interference fringes per x location, m, are calculated by the following equation:

$$m = \frac{2\delta}{\lambda} = \frac{2\delta}{\lambda^*}$$ (8)

where δ is the film thickness at x location, and λ is the wavelength of light in a vacuum. To calculate the wavelength of light in a thin film, λ^*, the following equation is required:

$$\lambda^* = \frac{\lambda}{n_f}$$ (9)

where λ is the wavelength of light and n_f is the refractive index of the film.

To characterize the light intensity of the light sources, reflection measurements on different samples were performed using the Edmund Optics 15x reflective objective described in Chapter 2. To accurately calibrate the reflectometer section of the instrument, reflection measurements of different materials were performed and then compared to literature results on those specific samples. Using four different light sources in the ultraviolet(UV), visible(Vis), and infrared(IR) range, it was feasible to obtain accurate measurements of reflection. Figure 10 below shows the wavelengths and intensities of these light sources.
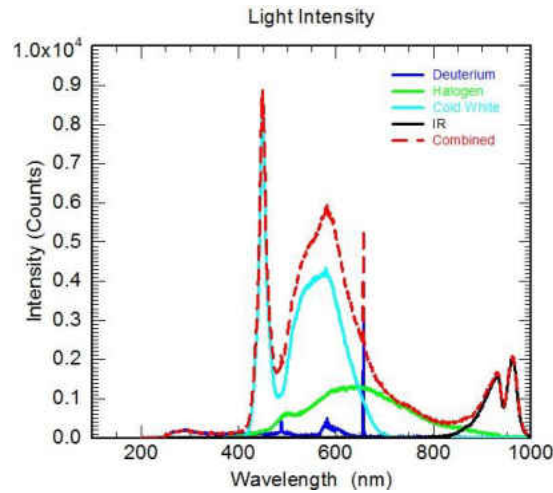
Figure 10: Intensity of individual light sources and combination of light sources

The intensity of these light sources is not the maximum intensity since the light is reflected and transmitted through different optics. Some of the optics are not 100% reflective and transmissive, therefore, there will be some light loss. To see interference fringes in an image, the light needs to be in the form of a single wavelength. Notice the two highest in peaks in Figure 10, they are at 450nm and at 656nm. These wavelengths, will be used to conduct experiments since there is a high intensity of light at these wavelengths. To perform a curvature profile experiment two bandpass filters were used. These bandpass filters let a single wavelength of light and blocks the wavelengths over and under this single wavelength. In this case, the one bandpass filter will let 450nm light pass and the other filter will let 656nm nm light pass through it. To fine tune the instrument, multiple reflection calibrations were conducted using Silicon (Si), Silicone Dioxide (SiO_2), Germanium (Ge), and Gold (Au) mirrors.
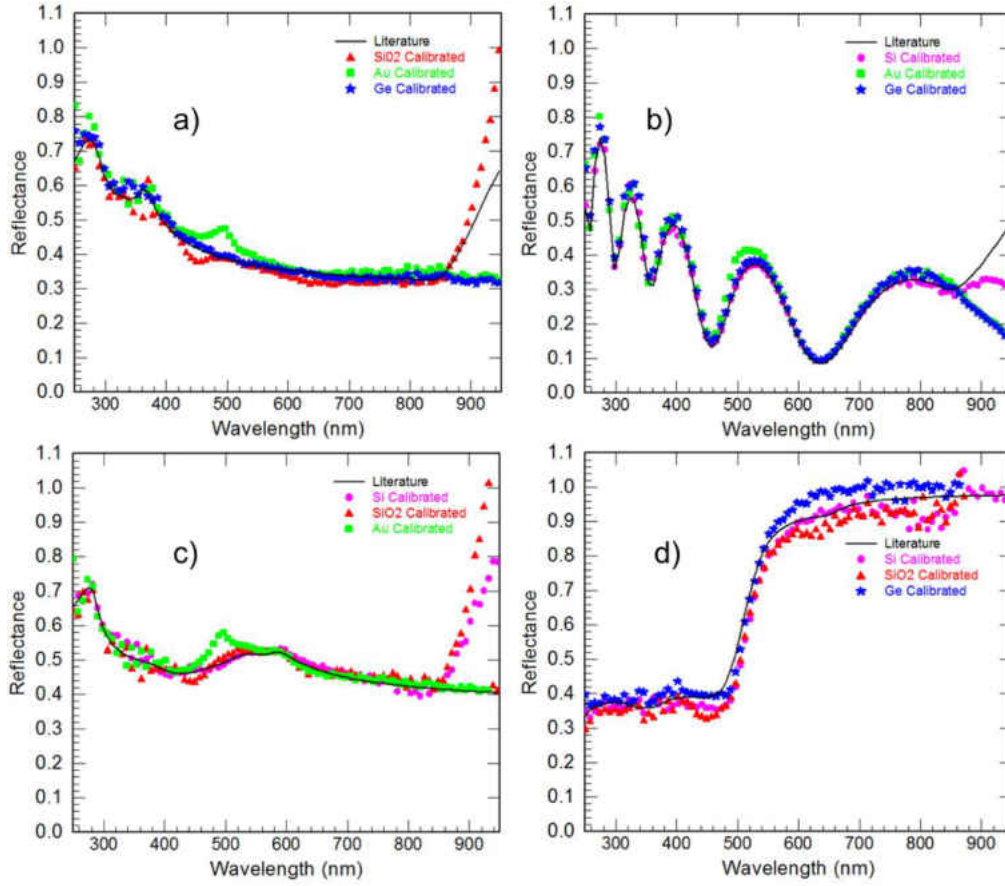
Figure 11: Calibration results of reflection (percent) of different materials compared to literature, where, a) Calibration of Si using SiO₂, Au, and Ge mirrors, b) Calibration of SiO₂ using Si, Au, and Ge, c) Calibration of Ge using Si, SiO₂, and Au mirrors, and d) Calibration of Au using Si, SiO₂, and Ge mirrors.

To characterize the reflection of this instrument, the light source intensity, $I_o(\lambda)$, was measured from the spectrometer reading the following equation was used:

$$I_o(\lambda) = \frac{I_m(\lambda)}{R_m(\lambda)} \qquad (10)$$

where $I_m(\lambda)$ is the reflected intensity of each material (m = Si, SiO₂, Ge, and Au), in the wavelength range λ (200nm – 1050nm) and $R_m(\lambda)$ in the literature results of the reflections of m materials. The calculated values were used for comparison between the calculated reflectance, $R_i(\lambda)$, using the light sources and literature results from each material using the following equation:

21

$$R_i(\lambda) = \frac{I_m(\lambda)}{[I_o(\lambda)]_n}, \text{when } m \neq n \qquad\qquad (11)$$

where $[I_o(\lambda)]_n$ is the computed intensity of the material, n, from the light source intensity. To show

that the spectrometer has been calibrated accurately, the reflection measurements of each material

using the intensity in the whole range are shown in Figure 11. Notice the reflection of SiO_2 using

the light source intensity range computed using Ge compared to the literature data of SiO_2 that

shows the accuracy of the Ge reflection, SiO_2 reflection, and spectrometer data. These calculations

confirm the precision of the spectrometer readings compared to literature data [21]–[23].

To analyze the curvature profile of a film, a code in MATLAB was developed. The

Mitutoyo 10x objective lens described in Chapter 2 is required for this analysis. Basically, the code

is an image analysis code. First, a grayscale image from the top of the samples is attained. The

grayscale image is then read by the code. Once the desired is image is selected, the user sets the

wavelength of light and the refractive index of the medium observed. Then, the user sets the region

of interest (ROI) for analysis by selecting, the height from the top of the image, the width of the

ROI's left side from left side, the width of the right side of the ROI from the left side. Once the

ROI is selected, the thickness of the ROI is averaged for accurate analysis. After the ROI is

selected, the code reads the grayscale values of the image for 0 being black to 255 being white.

The code then plots the gray values as a function of x position. Once the gray values are plotted,

the MATLAB function find peaks is used to find all the maximum peaks. Once all the peaks are

found, the code plots the peaks to their corresponding locations on the grayscale curve. Since the

curvature changes as a x changes, the fringes in the image change as a function of x, meaning that

the spacing between the fringes will change as x changes. From the plotted peaks, the code makes

a curve fit to frequency data for auto interpolation from the distance between these peaks. Once

the peaks are plotted, the code takes that frequency plot and makes a plot of the angle per pixel location. Finally, the code takes the angle plot and makes a new plot of the thickness of the film per pixel location in which this plot is the curvature profile of the analyzed film. The Figures below show an example of the necessary steps and inputs to accurately analyze the curvature profile of a film. To show the necessary steps on how the developed code runs Lens$_1$ will be observed.
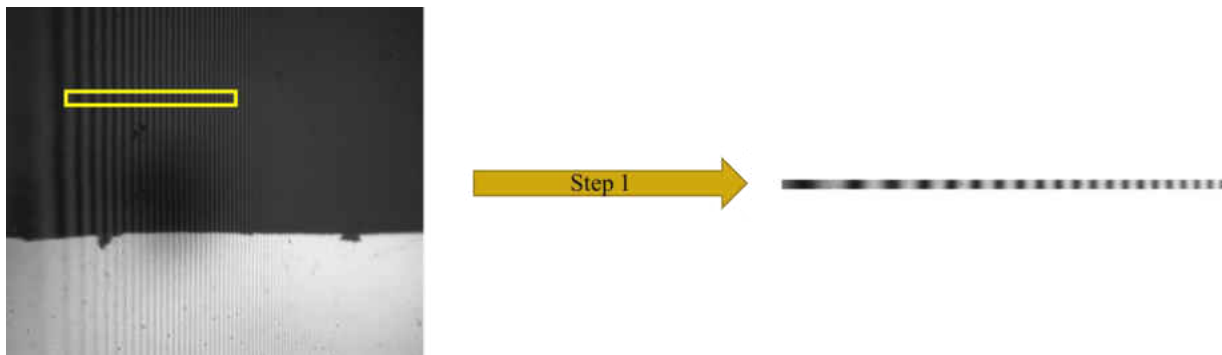
Figure 12: Step 1, (Left) Gray value image of Lens$_1$ interference at a wavelength of 656nm, (Right) Selected region of interest.

The inputs for this example are designated as follows, the first step is to set the wavelength of light, λ, is set to 656nm since the light used is 656nm, and the refractive index of the medium, n_f, is set to 1.005 since the film observed is air. To select the size of the ROI the height from the top of the image is set to 30%, the start of width from the left is set to 10% from the left of the image, the width end is set to 30% from the left of the image and the thickness of the region of interest is set to 20 pixels. Note, the gray values of the 20 pixels selected for the thickness of the ROI are averaged in the vertical direction to one single line of pixels for better accuracy and less noise.

Figure 13: Step 2, (Left) Selected region of interest of gray value image, (Right) Plot of the gray values as a function of position (*x*).

In step 2, the code take the region of interest and plots the gray values as a function of position (*x*). To plot the gray values, the code reads the gray values of the ROI in a scale of 0 being completely black and 255 being completely white.
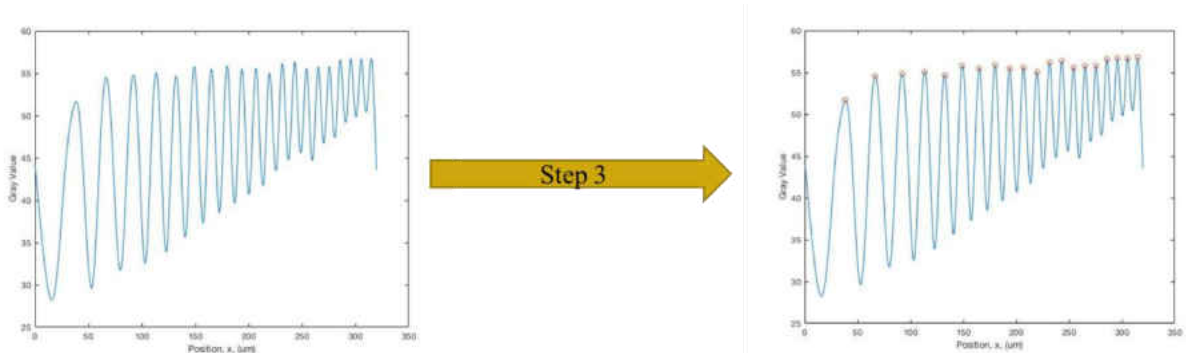
Figure 14: Step 3, (Left) Plot of the gray values as a function of position(*x*), (Right) Peaks plotted to corresponding locations on grayscale curve.

In step 3, the MATLAB function find peaks is used to find the maximum peaks of the gray values plot. Notice that the frequency of the peaks increases as *x* increases, this means that as *x* increases the frequency increases, this is due to the curvature of the air film caused by the curvature of the lens.

24

Figure 15: Step 4, (Left) Peaks plotted to corresponding locations on grayscale curve, (Right) Curve fit to interpolate frequency data for auto-interpolation.

In step 4, once the peaks are plotted to their corresponding locations on a grayscale curve, the code creates a plot, which curve fits the peaks to frequency. To create the frequency vs position (um) the MATLAB code reads the following equation:

$$f_i = \frac{1}{LocPeak_{i+1} - LocPeak_i} \qquad (12)$$

where, f_i, is the frequency per micron (um), $LocPeak_i$ is the x location of the local peak, $LocPeak_{i+1}$ is the x location of the next peak. Notice that in the left axis the real frequency data starts at 0.02, this is because at the point of contact ($x = 0$) Equation 4 is undefined since the angle is zero and it is in the bottom of the denominator. Since we have a constant curvature lens, the change in the angle is directly proportional to the change in x direction, therefore, it can be said that the frequency starts at zero since where the frequency start is close to zero. This statement takes care of the undefined point. The yellow line is the frequency starting at zero.
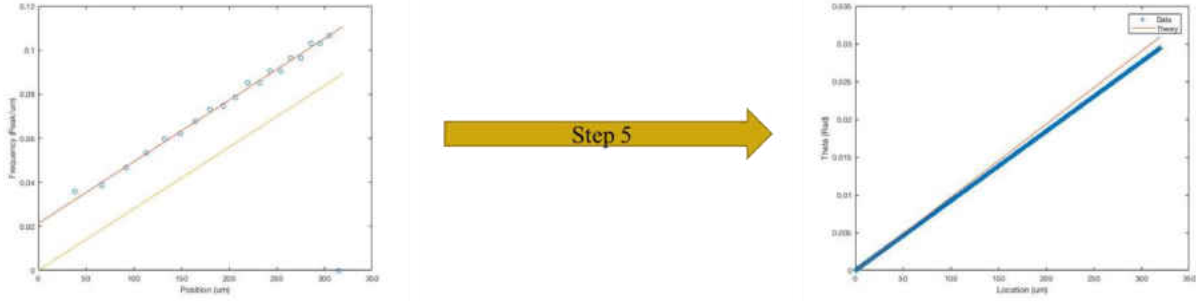
Figure 16: Step 5, (Left) Curve fit to frequency data for auto-interpolation, (Right) Plot of angle (θ) per pixel location (x).

In step 5, the MATLAB code takes the frequency plot and converts it to a plot of theta (in radians) vs pixel location (x) using the following equations:

$$\theta_i = \frac{f_i \lambda^*}{2} \qquad (13)$$

where, θ_i is the angle of curvature of the lens and an specific x location, f_i is the frequency per micron, and λ^* is the wavelength of light of the observed medium. The following equation is used to find λ^* [19]:

$$\lambda^* = \frac{\lambda}{n_f} \qquad (14)$$

where, λ is the wavelength of light in a vacuum, and n_f is the refractive index of the film observed.
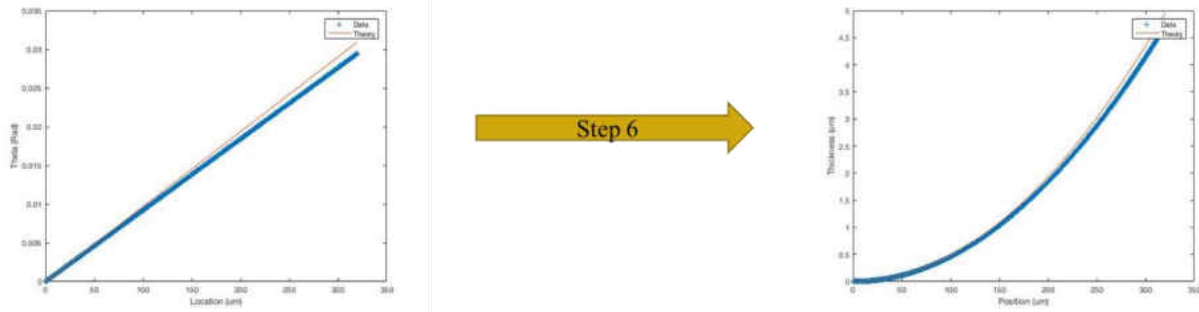
Figure 17: Step 6, (Left) Plot of the angle (θ) per pixel (x) location, (Right) Thickness (δ) of film per pixel (x) location.

Finally, in step 6 the code converts the plot of the angle per pixel location into the thickness profile of the film using the following equation:

$$\delta_i = \delta_{i-1} + tan(\theta_i)\, dx \qquad\qquad (\,15\,)$$

where, δ_i is the height of the grayscale location, δ_{i-1} is the height of the previous grayscale value location, θ_i is the angle of curvature of the observed film at a specific location, and dx is the pixel width in microns. This equation shows the curvature profile and the thickness at a specific x location of the analyzed film.

Settings and constants

The table below shows the input values used to analyze Lens$_1$, Lens$_2$, and Lens$_3$ using the same steps shown in the previous formulas section. This experiment will be conducted using a 10x reflective objective.

Table 1:Inputs used for each lens analysis

Samples	Refractive index (n_f)	Wavelengths (λ)	dx (10x Objective)	Pixels to average
Lens 1	1.005 (air film)	450nm, 656nm	0.335	20
Lens 2	1.005 (air film)	450nm, 656nm	0.335	20
Lens 3	1.005 (air film)	450nm, 656nm	0.335	20

The samples observed are the three lenses described in the experiment materials chapter. The refractive index selected was 1.005 since the film observed is air. The two wavelengths used were 450nm and 656nm because that is where the light has the most intensity. The objective lens used was the 10x objective described in the experimental materials chapter with a pixel width of 0.335. The pixels to average was set to 20 for all samples for consistency.

<u>Images and Analysis</u>

A total of six pictures were obtained for to conduct the curvature profile experiment of the three different lenses described in the experimental materials section. The following images will show the grayscale images, the ROI observed, and the curvature profile analysis compared to literature.

Figure 18: ROI's of grayscale images of Lens₁, (Left) taken at a wavelength of 450nm, (Right) taken at a wavelength of 656nm.

Figure 18 shows the grayscale images of Lens₁ at different two different wavelengths, notice that frequency of the fringes at 450nm is larger than the frequency of the fringes at 650nm. This cylindrical lens has the greatest frequency since it has the largest curvature. This is related to Equation 4 which shows that separation between fringes is larger if the wavelength is larger because λ is in the numerator. As a result, if λ is larger, the spacing between fringes is smaller, therefore the fringe frequency is larger. This cylindrical lens has the greatest frequency and smallest fringe spacing since it has the largest curvature, meaning that as the angle changes as a function of *x*, the thickness of the air fill will increase faster in the *x* direction faster than the other two lenses.
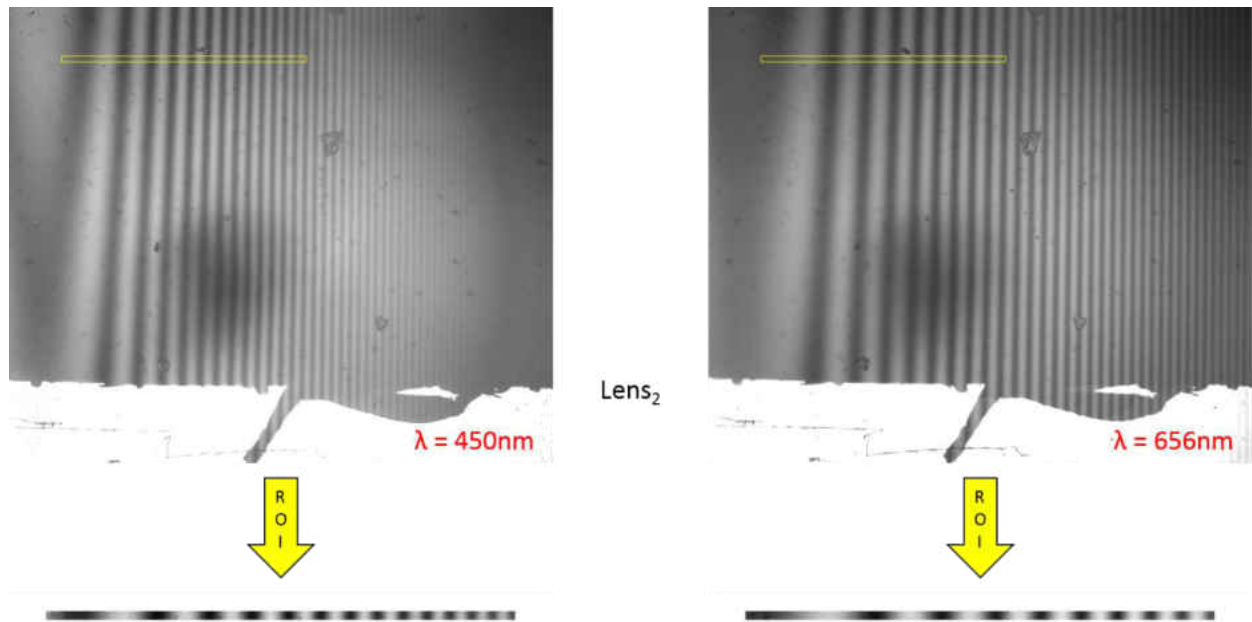
Figure 19: ROI's of grayscale images of Lens$_2$, (Left) taken at a wavelength of 450nm, (Right) taken at a wavelength of 656nm.

Figure 19 shows the grayscale images of Lens$_2$ at different two different wavelengths, notice that frequency of the fringes at 450nm is larger than the frequency of the fringes at 650nm. This is explained in the previous page beneath Figure 18. This cylindrical lens has the medium fringe frequency and medium fringe spacing since it its curvature is in between Lens$_1$ and Lens$_3$. This cylindrical lens has the medium frequency since it has the medium curvature, meaning that as the angle changes as a function of *x*, the thickness of the air film will increase slower than Lens$_1$ and faster than Lens$_3$ in the *x* direction.
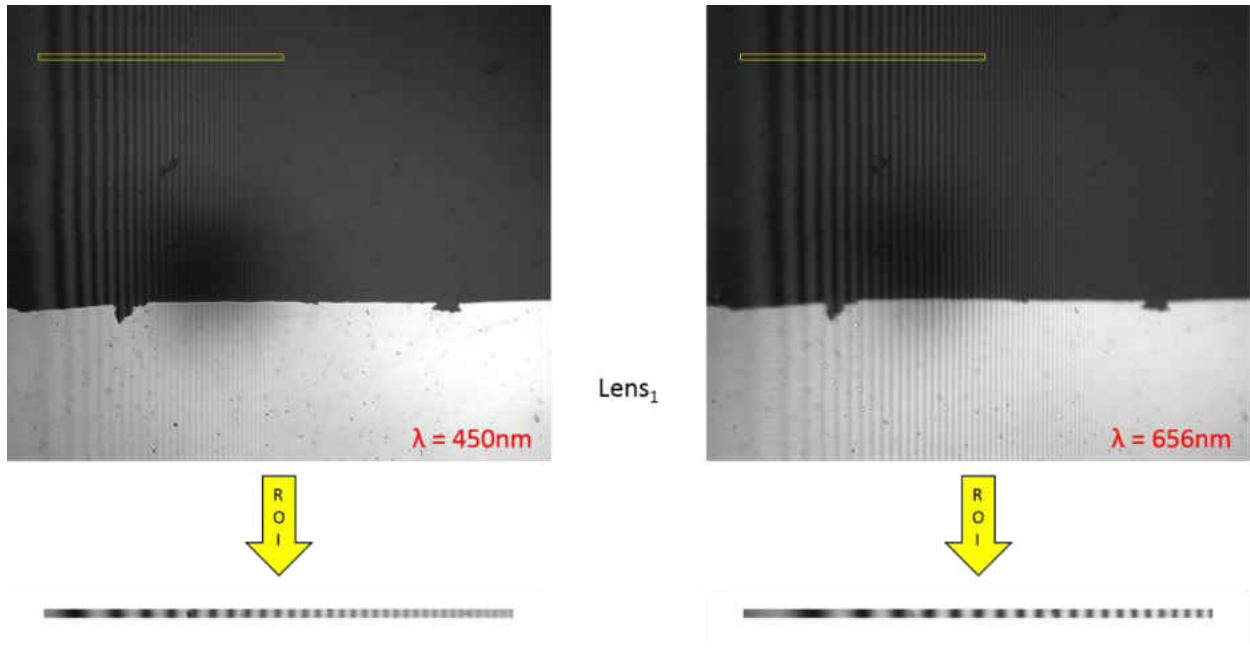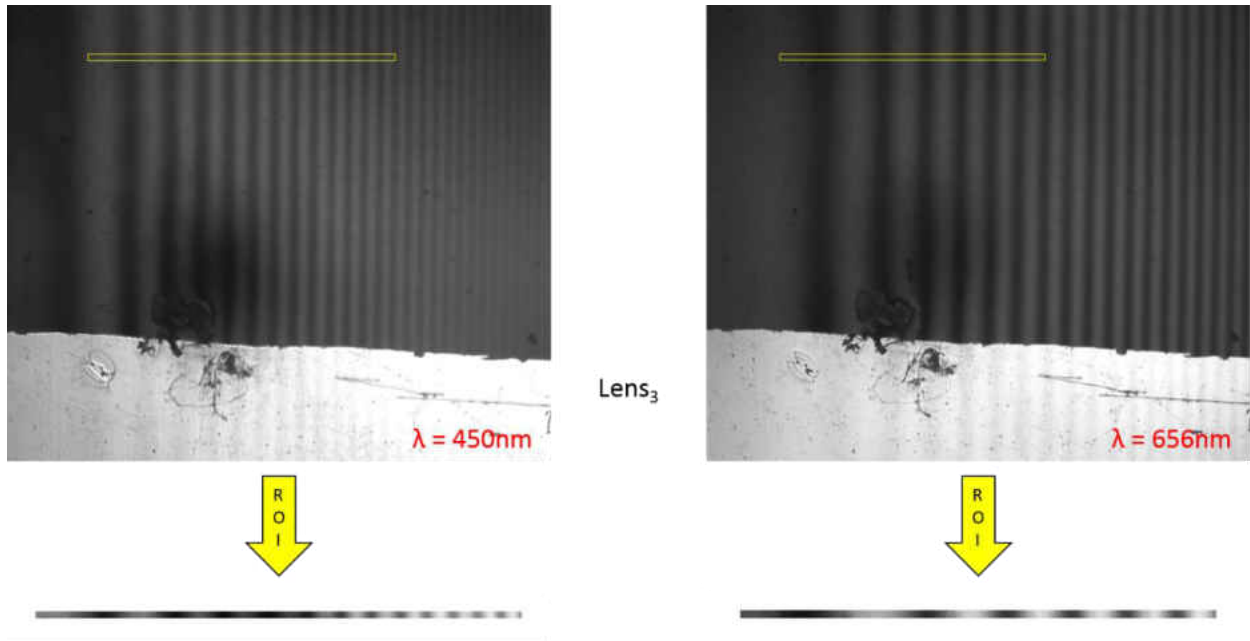
Figure 20: ROI's of grayscale images of Lens₃, (Left) taken at a wavelength of 450nm, (Right) taken at a wavelength of 656nm.

Figure 19 shows the grayscale images of Lens₃ at different two different wavelengths, notice that frequency of the fringes at 450nm is larger than the frequency of the fringes at 650nm. This is explained in the paragraph under Figure 18. This cylindrical lens has the smallest frequency since it its curvature is the smallest curvature of all lenses. This cylindrical lens has the smallest fringe frequency and largest fringe spacing since it has the smallest curvature, meaning that as the angle changes as a function of x, the thickness of the air film in the x direction will increase slower than Lens₁ and Lens₂.
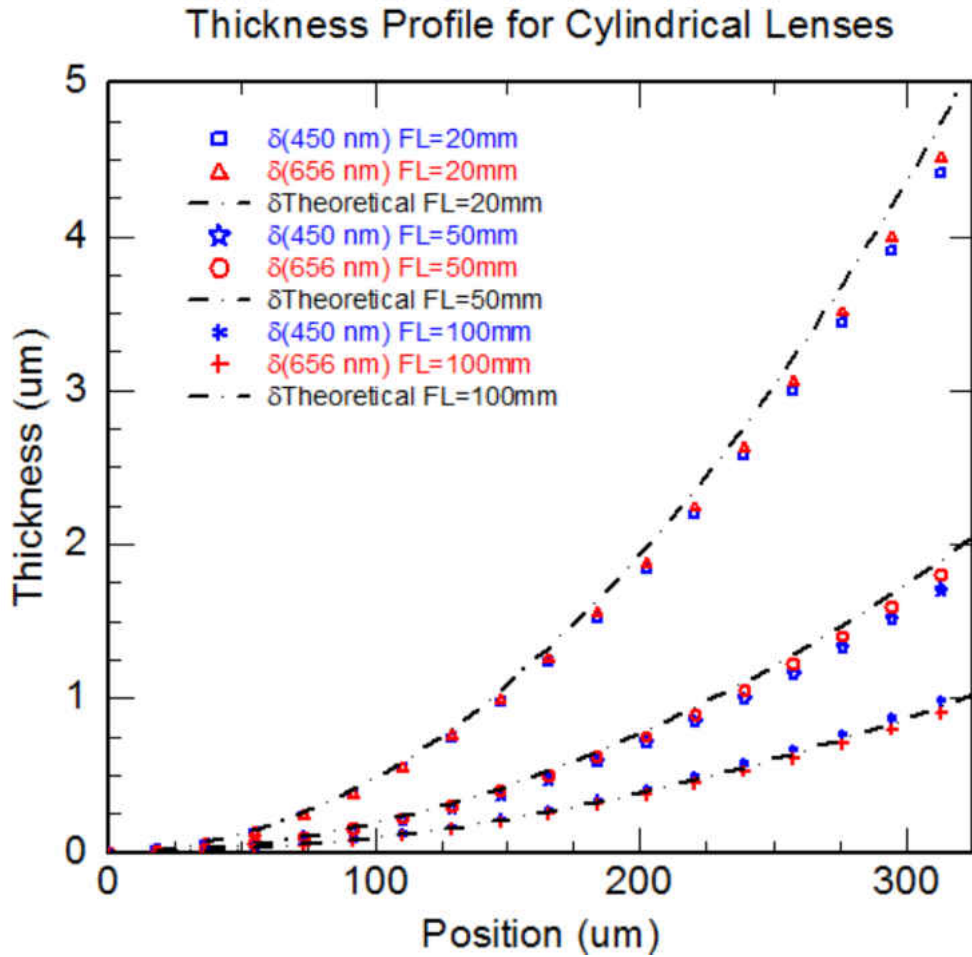
Figure 21: (Top) ROI's observed of the three different lenses at 450nm and 656nm, (Bottom) Thickness profiles of cylindrical lenses observed as a function of position.

Table 2: Inputs and error calculations

Samples	Refractive index (n_f)	Wavelengths (λ)	dx (10x Objective)	Pixels to average	450nm Error	656nm Error
Lens 1	1.005 (air film)	450nm, 656nm	0.335	20	7.7%	5.7%
Lens 2	1.005 (air film)	450nm, 656nm	0.335	20	10.8%	5.9%
Lens 3	1.005 (air film)	450nm, 656nm	0.335	20	4.1%	5.6%

As expected, the results shown in Figure 21 match the theoretical (black dashed line) data. Notice that the largest error is from $Lens_2$ with a 10.8% error. Observing the ROI at 450 nm selected from $Lens_2$, about 25% in the ROI from left to right, there is an imperfection in the picture. This imperfection could be a dust particle in the samples, optics or camera. These errors would be a lot lower if the experiment were to be performed in a clean room, where there would be less contaminants in the samples or optics. Another factor that can be considered in these errors is the camera resolution. At this size scale, a camera with more pixel resolution could have acquired better images, therefore resulting in a better image quality for analysis.

Notice the ROI's at the top, the fringes in $Lens_1$ have the smallest separation between fringes because the curvature profile is larger than $Lens_2$ and $Lens_3$. The spacing between the fringes from $Lens_1$ ROI are analyzed in the MATLAB code confirming that the thickness of the air film in $Lens_1$ will increase faster than $Lens_2$ and $Lens_3$, showing a steeper curvature profile. The thickness profile plot shows that the curvature profile of $Lens_1$ is larger than $Lens_2$ and $Lens_3$.

Notice the ROI's at the top, the fringes in $Lens_2$ have the medium separation between fringes because the curvature profile is in between $Lens_1$ and $Lens_3$. The spacing between the fringes from $Lens_2$ ROI are analyzed in the MATLAB code confirming that the thickness of the air film in $Lens_1$ will increase at a medium rate between $Lens_1$ and $Lens_3$. The thickness profile plot shows that the curvature profile of $Lens_2$ is in between $Lens_1$ and $Lens_3$.

Notice the ROI's at the top, the fringes in $Lens_3$ have the largest separation between fringes because the curvature profile is smaller $Lens_1$ and $Lens_2$. The spacing between the fringes from $Lens_3$ ROI are analyzed in the MATLAB code confirming that the thickness of the air film in $Lens_3$

will increase at a slower rate than $Lens_1$ and $Lens_2$. The thickness profile plot shows that the curvature profile of $Lens_3$ is smaller than $Lens_1$ and $Lens_2$.

CHAPTER 5: CONCLUSIONS

Overview

A new technique is accessible for simultaneous measurements of solid and liquid films using a single instrument. This work combines a reflectometer with an interferometer for simultaneous thin film measurements. In previous studies, thin films and curvature measurements are conducted by either a reflectometer or an interferometer independently, but not simultaneously [24]–[29]. A combination of both, a CCD camera for grayscale images to measure interference fringes and a spectrometer to measure the reflection of a thin film, simplifies the curvature measurements of different films.

Figure 1 shows the optical setup of the instrument. This instrument consists of two different light sources with two different lights in them. The first light source emits deuterium UV light and a tungsten halogen light emits visible light. The other light source consists of a cold white light which emits light in the visible range and a light emitting diode which emits IR light. Combining these lights together a wide range of the spectrum can be observed. These lights are merged together into an optical fiber that takes the lights from the two light sources and merges the together into a single fiber that emits the combined lights. Once the light comes out of the fiber, it is reflected on a parabolic mirror that collimates the light. Once the light is collimated, it reflects on a 50/50 beam splitter into a 10x objective lens. The objective lens focuses the light and the camera image at the same time in to the sample. Once the light reflects from the sample it travels through the objective lens and the beam splitter into a lens that focuses the light into a fiber that guides the light into the spectrometer for flat thin films measurements. A CCD camera with an

interchangeable lens holder, which holds a bandpass filter in the 450nm range and another bandpass filter at 656nm, is used to shine single wavelength light (450nm or 656nm light) into the sample since single wavelength light is needed to see interference fringes of films at different angles. After the bandpass filters there is an achromatic les that focuses the camera image into the sample. A silver (Ag) mirror reflects an image from the sample thorough the beam splitter and objective.

A code developed using MATLAB software is used for image analysis. The fringes in the grayscale images acquired from the camera are read by the code. Once the image is loaded in the code, the user sets the parameters to select a region of interest. Once the region of interest is selected, the code reads the gray values and plots the gray values as a function of distance. Using the find peaks function in MATLAB, the peaks of the grayscale values are selected. Once the peaks are selected, the distance between the peaks is measured, which come from the spacing between the fringes, the code plot a linear fit of the frequency as a function of position. Once the frequency of the peaks is plotted, the code plots the angle at the specific location as a function of pixel location *x*. Finally, once the angle per pixel location is plotted, the code plots the thickness of the film per *x* location. The thickness of the film per pixel location shows the curvature profile of a film like it is shown in the results.

Characterization of diverse curved lenses to create a curved film of air using reflection and interferometry, show the expected results of these lenses curvature profiles. The results show quality readings from the grayscale image to obtain curvature profiles of films. In this case, the medium used for analysis is air. The advantage of this instrument and code is that curvature

measurements can be made with ease by changing a few inputs for different mediums other than air. This instrument facilitates the analysis of liquids meniscus curvature profiles and can be used to measure heat transfer properties of different types of films of air, liquid, and solid surfaces. The liquid meniscus region is important due to its heat transfer characteristics. Modifying the liquid meniscus can result in better cooling for devices that are limited by heat.

<u>Future work</u>

This instrument will be used in the studies of wicking structures introduced in heat pipes. These wicking structures drive the fluid towards a heated section without the use of external mechanisms or devices. These wicking structures decrease the chance of a region drying out due to the fluid motion caused towards a dry region. Using this instrument to characterize a liquid meniscus facilitates the analysis of high wetting fluids used in heat pipes.

APPENDIX: MATLAB ALGORITHM CODE

```
clear all
ZerOrdFring = 0;%um
PxDist = 0.335 ;

n_meniscus = 1.005;
prompt = 'What image would you like to use? : '
IMAGE = input(prompt);
Img = imread(IMAGE);%Read image
Lambda = input('What Wavelength of light are you using? (um) : ')/1000; %um
rev = 0;                %1 reverses image, 0 remains same
IMG = REV_IMG(rev,Img);        %new image depending on reveral parameter
[m,n] = size(IMG);          %Declare Rows and Columns image size
x = 1:1:n;              %x (Start value, Step, End)
y = 1:1:m;  %y (Start value, Step, End)
imshow(Img)
Top = input('What percentage of height would you like to start the image? (0 = top) : ');
Left = input('What percentage of width would you like to start the image? (0 = left) : ');
Right = input('What percentage of width would you like to end the image? (0 = left) : ');
Thick = input('How many pixels would you like to average? : ');
Y = Top/100+1/100;            %Height of top part
th = Thick;            %Thickness of slice of img
ls = Left/100+1/100;              %Distance from left
rs = Right/100;            %Distance from left
z = 1;            %Pixels per calculation EOP
   u = round(n*(ls));
   v = round(n*(rs));
   w = (u:z:v);            %width
   a = round(u/z);            %Round for index
   b = round(v/z);            %Round for index
   h = round(m*Y);             %Gray height line reading
   X = a:1:b;              %rounded values of interval UV
   FR = double(IMG(h:h+th-1,w)); %Read fringes at that height
   VIEW = IMG(h:h+th-1,w);      %View picture of fringe section


%RGB = insertShape(IMG, 'rectangle', [round(n*rs) h round(n*(ls-rs)) th], 'Linewidth',5);
   %RGB = REV_IMG(rev,RGB);
FRavg = zeros(1,b-a+1);      %Average of slices int
FRavg = zeros(1,b-a+1);      %Average of slices int
for i=1:1:th            %Signal average
   FRavg = FRavg + FR(i,:);
   if i==th
      FRavg = FRavg/th;
      break;
   end
end

alpha = 0.45;
FRfilt = filter(alpha,[1 alpha - 1],FRavg);
FRfilt = sgolayfilt(FRavg, 1, 21);
[Gmax, Gmin] = envelope (FRfilt);
X=X*PxDist;
[ll,kk]=size(X);
DX = 0:PxDist:PxDist*(kk-1);
GBAR = Gbar(FRfilt,Gmin,Gmax);
GBfilt = sgolayfilt(GBAR, 3, 101);

[pks,locs] = findpeaks(FRfilt,DX);
[xxx,Numpeaks] = size(locs);
f = zeros(1,Numpeaks);
for i=1:1:Numpeaks-1
```

```matlab
    f(1,i) = ((locs(1,i+1)-locs(1,i)))^(-1);
end

ord = 1;
Start = 4;
End = 25;
fringecheck=1;


while fringecheck==1
    p = polyfit(locs(1,Start+1:Numpeaks-End),f(1,Start+1:Numpeaks-End),ord);
    Frq2 = polyval(p,DX);
    p(1,ord+1)=0;
    Frq = polyval(p,DX);
    figure(01)
    for i = Start+1:1:Numpeaks-End
    plot(locs(1,i),f(1,i),'o')
    hold on
    end
    plot(DX,Frq2);
prompt = 'Is this frequency plot good? Y/N (1,0):  ';
checker = input(prompt);
if checker==0
    fringcheck=1;
    Start = input('How many fringes would you like to skip from the front?  ');
    End = input('How many fringes would you like to skip from the end?  ');
    ord = input('What order polynomial would you like to use?  ');
elseif checker==1
    fringecheck=0;
else
    fringcheck = 1;
end
close all;
end
```

REFERENCES

[1]   J. M. Wraith and D. Or, "Temperature effects on soil bulk dielectric permittivity measured by time domain reflectometry: Experimental evidence and hypothesis development," *Water Resour. Res.*, vol. 35, no. 2, pp. 361–369, Feb. 1999.

[2]   G. C. Topp and J. L. Davis, "Measurement of Soil Water Content using Time-domain Reflectometry (TDR): A Field Evaluation1," *Soil Sci. Soc. Am. J.*, vol. 49, no. 1, p. 19, 1985.

[3]   D. Moret, J. L. Arrúe, M. V. López, and R. Gracia, "A new TDR waveform analysis approach for soil moisture profiling using a single probe," *J. Hydrol.*, vol. 321, no. 1–4, pp. 163–172, Apr. 2006.

[4]   K. A. Koye and W. O. Winer, "An Experimental Evaluation of the Hamrock and Dowson Minimum Film Thickness Equation for Fully Flooded EHD Point Contacts," *J. Tribol.*, vol. 103, no. 2, p. 284, Apr. 1981.

[5]   R. K. Heilmann, C. G. Chen, P. T. Konkola, and M. L. Schattenburg, "Dimensional metrology for nanometre-scale science and engineering: towards sub-nanometre accurate encoders," *Nanotechnology*, vol. 15, no. 10, pp. S504–S511, Oct. 2004.

[6]   N. Bobroff, "Recent advances in displacement measuring interferometry," *Meas. Sci. Technol.*, vol. 4, no. 9, pp. 907–926, Sep. 1993.

[7]   G. Beheim, "Fiber-optic interferometer using frequency-modulated laser diodes," *Appl. Opt.*, vol. 25, no. 19, p. 3469, Oct. 1986.

[8]   *,† Mathias Lösche, ‡ Johannes Schmitt, ‡,§ Gero Decher, ‖,⊥ and Wim G. Bouwman, and

K. Kjaer‖, "Detailed Structure of Molecularly Thin Polyelectrolyte Multilayer Films on Solid Substrates as Revealed by Neutron Reflectometry," 1998.

[9] A. Rosencwaig, J. Opsal, D. L. Willenborg, S. M. Kelso, and J. T. Fanton, "Beam profile reflectometry: A new technique for dielectric film measurements," *Appl. Phys. Lett.*, vol. 60, no. 11, pp. 1301–1303, Mar. 1992.

[10] M. H. W. Hendrix, R. Manica, E. Klaseboer, D. Y. C. Chan, and C.-D. Ohl, "Spatiotemporal Evolution of Thin Liquid Films during Impact of Water Bubbles on Glass on a Micrometer to Nanometer Scale," *Phys. Rev. Lett.*, vol. 108, no. 24, p. 247803, Jun. 2012.

[11] V. S. Alahverdjieva, K. Khristov, and D. Exerowa, "Correlation between adsorption isotherms, thin liquid films and foam properties of protein/surfactant mixtures: Lysozyme/C10DMPO and lysozyme/SDS," *Colloids Surfaces A Physicochem. Eng. Asp.*, vol. 323, no. 1, pp. 132–138, 2008.

[12] J. . Israelachvili, "Thin film studies using multiple-beam interferometry," *J. Colloid Interface Sci.*, vol. 44, no. 2, pp. 259–272, Aug. 1973.

[13] W. M. Nozhat, "Measurement of liquid-film thickness by laser interferometry.," *Appl. Opt.*, vol. 36, no. 30, pp. 7864–9, Oct. 1997.

[14] R. Ohmura, S. Kashiwazaki, and Y. H. Mori, "Measurements of clathrate-hydrate film thickness using laser interferometry," *J. Cryst. Growth*, vol. 218, no. 2, pp. 372–380, 2000.

[15] S. A. Putnam, A. M. Briones, J. S. Ervin, M. S. Hanchak, L. W. Byrd, and J. G. Jones, "Interfacial heat transfer during microdroplet evaporation on a laser heated surface," *Int. J. Heat Mass Transf.*, vol. 55, no. 23, pp. 6307–6320, 2012.

[16] S. A. Putnam *et al.*, "Microdroplet evaporation on superheated surfaces," *Int. J. Heat Mass*

Transf., vol. 55, no. 21, pp. 5793–5807, 2012.

[17]   M. Mehrvand and S. A. Putnam, "Heat transfer coefficient measurements in the thermal boundary layer of microchannel heat sinks," in *2016 15th IEEE Intersociety Conference on Thermal and Thermomechanical Phenomena in Electronic Systems (ITherm)*, 2016, pp. 487–494.

[18]   S. S. Panchamgam, J. L. Plawsky, and P. C. Wayner, "Microscale heat transfer in an evaporating moving extended meniscus," *Exp. Therm. Fluid Sci.*, vol. 30, no. 8, pp. 745–754, 2006.

[19]   P. A. Tipler, *Physics for scientists and engineers*. Worth Publishers, 1991.

[20]   M. V. Klein and T. E. (Thomas E. Furtak, *Optics*. Wiley, 1986.

[21]   P. B. Johnson and R. W. Christy, "Optical Constants of the Noble Metals," *Phys. Rev. B*, vol. 6, no. 12, pp. 4370–4379, Dec. 1972.

[22]   I. H. Malitson, "Interspecimen Comparison of the Refractive Index of Fused Silica*,†," *J. Opt. Soc. Am.*, vol. 55, no. 10, p. 1205, Oct. 1965.

[23]   D. E. Aspnes and A. A. Studna, "Dielectric functions and optical parameters of Si, Ge, GaP, GaAs, GaSb, InP, InAs, and InSb from 1.5 to 6.0 eV," *Phys. Rev. B*, vol. 27, no. 2, pp. 985–1009, Jan. 1983.

[24]   M. Foster, M. Stamm, and G. Reiter, "X-ray reflectometer for study of polymer thin films and interfaces," *Vacuum*, vol. 41, no. 4–6, pp. 1441–1444, Jan. 1990.

[25]   A. L. Kholkin, C. Wütchrich, D. V. Taylor, and N. Setter, "Interferometric measurements of electric field-induced displacements in piezoelectric thin films," *http://oasc12039.247realmedia.com/RealMedia/ads/click_lx.ads/www.aip.org/pt/adcenter*

/pdfcover_test/L-37/1696128366/x01/AIP-

PT/RSI_ArticleDL_032917/APRconf_1640x440Banner_12-

16B.jpg/434f71374e315a556e61414141774c75?x, 1998.

[26] W. Fang, H.-C. Tsai, and C.-Y. Lo, "Determining thermal expansion coefficients of thin films using micromachined cantilevers," *Sensors Actuators A Phys.*, vol. 77, no. 1, pp. 21–27, 1999.

[27] J. T. Fanton, J. Opsal, D. L. Willenborg, S. M. Kelso, and A. Rosencwaig, "Multiparameter measurements of thin films using beam-profile reflectometry," *J. Appl. Phys.*, vol. 73, no. 11, pp. 7035–7040, Jun. 1993.

[28] K. Manoli, D. Goustouridis, S. Chatzandroulis, I. Raptis, E. S. Valamontes, and M. Sanopoulou, "Vapor sorption in thin supported polymer films studied by white light interferometry," *Polymer (Guildf).*, vol. 47, no. 17, pp. 6117–6122, 2006.

[29] H. Zhang, J. W. Lynn, C. F. Majkrzak, S. K. Satija, J. H. Kang, and X. D. Wu, "Measurements of magnetic screening lengths in superconducting Nb thin films by polarized neutron reflectometry," *Phys. Rev. B*, vol. 52, no. 14, pp. 10395–10404, Oct. 1995.